Protein Science (1995), *4*:716–728. Cambridge University Press. Printed in the USA.

Secondary and tertiary structure of the A-state of cytochrome *c* from resonance Raman spectroscopy

TRACE JORDAN, JANINA C. EADS,[1] AND THOMAS G. SPIRO
Department of Chemistry, Princeton University, Princeton, New Jersey 08544

(RECEIVED October 4, 1994; ACCEPTED January 23, 1995)

Abstract

Ferricytochrome *c* can be converted to the partially folded A-state at pH 2.2 in the presence of 1.5 M NaCl. The structure of the A-state has been studied in comparison with the native and unfolded states, using resonance Raman spectroscopy with visible and ultraviolet excitation wavelengths. Spectra obtained with 200 nm excitation show a decrease in amide II intensity consistent with loss of structure for the 50s and 70s helices. The 230-nm spectra contain information on vibrational modes of the single Trp 59 side chain and the four tyrosine side chains (Tyr 48, 67, 74, and 97). The Trp 59 modes indicate that the side chain remains in a hydrophobic environment but loses its tertiary hydrogen bond and is rotationally disordered. The tyrosine modes Y8b and Y9a show disruption of tertiary hydrogen bonding for the Tyr 48, 67, and 74 side chains. The high-wavenumber region of the 406.7-nm resonance Raman spectrum reveals a mixed spin heme iron atom, which arises from axial coordination to His 18 and a water molecule. The low-frequency spectral region reports on heme distortions and indicates a reduced degree of interaction between the heme and the polypeptide chain. A structural model for the A-state is proposed in which a folded protein subdomain, consisting of the heme and the N-terminal, C-terminal, and 60s helices, is stabilized through nonbonding interactions between helices and with the heme.

Keywords: A-state; cytochrome *c*; resonance Raman

Partially folded states of proteins are interesting systems for studying the molecular interactions that stabilize polypeptide structure (Dill & Shortle, 1991). Ptitsyn (1986) proposed the term "molten globule" to designate a partially folded protein that exhibits a reduced degree of secondary and tertiary structure relative to the native conformation, and in a recent review he reports the observation of molten globules for 18 different proteins (Ptitsyn, 1993). Molten globules can be produced by varying solvent pH, ionic strength, and denaturant concentration or through modifications of the protein sequence (Kuwajima, 1989; Christensen & Pain, 1991, 1994; Bychkova & Ptitsyn, 1994). The structure of the molten globule often consists of a protein subdomain that is stabilized via hydrophobic interactions. In α-lactalbumin, for example, the B- and C-helices are stabilized through nonpolar interactions (Chyan et al., 1993), whereas in apomyoglobin the folded subdomain consists of the A-, G-, and H-helices (Hughson et al., 1990). Molten globules are also interesting models for understanding the dynamics of protein folding because for α-lactalbumin and myoglobin they closely resemble the structure of kinetic folding intermediates (Ikeguchi et al., 1986; Jennings & Wright, 1993).

Horse heart cytochrome *c* (cyt *c*) is a useful protein for comparing the structures of different equilibrium folding states. The native protein (N-state) contains 104 amino acids, with a secondary structure consisting of five α-helices and six β-turns (Bushnell et al., 1990). Its physiological role as a redox protein requires a heme prosthetic group, which is mostly buried in the hydrophobic core of the polypeptide chain (Dickerson & Timkovich, 1975; Timkovich, 1979). Cyt *c* can be unfolded at pH 2 in the absence of salt (U-state). However, the protein can also form a partially folded state, called the A-state, under very acidic conditions (pH < 2) or at pH 2 in the presence of 0.5–1.5 M NaCl or KCl (Fink et al., 1990; Goto et al., 1990a; Jeng et al., 1990; Jeng & Englander, 1991). The A-state structure is stabilized because the salt ions screen the repulsive electrostatic interactions that occur upon protonation of carboxylate side chains (Goto et al., 1990b; Goto & Nishikiori, 1991; Stigter et al., 1991).

The structure of A-state cyt *c* has been extensively studied using several experimental techniques. Small angle X-ray scattering experiments indicate that the A-state is globular and compact, with a radius of gyration of 17.4 Å compared to 13.5 Å for the native protein (Kataoka et al., 1993). Calorimetric measurements of ΔC_p for unfolding, which largely reflects the hy-

Reprint requests to: Thomas G. Spiro, Department of Chemistry, Princeton University, Princeton, New Jersey 08544; e-mail: spiro@chemvax.princeton.edu.
[1] Present address: Department of Biochemistry, Albert Einstein College of Medicine, Bronx, New York 10461.

dration of nonpolar groups, obtained values of 5.34 and 1.79 kJ/K·mol for the N- and A-states, respectively; the A-state value is reduced because some interior hydrophobic residues have already become exposed to solvent in the molten globule (Kuroda et al., 1992; Hagihara et al., 1994). Studies of tryptophan fluorescence, which is strongly quenched for the native protein, showed only a small increase in quantum yield for the A-state, suggesting that the single Trp 59 side chain remains close to the heme as required for efficient energy transfer (Jeng & Englander, 1991). However, near-UV CD spectroscopy showed a reduction in ellipticity at 280 nm, which indicates conformational disorder for Trp 59 in the A-state (Goto & Nishikiori, 1991). The CD ellipticity at 222 nm was used to calculate a small reduction in helical content from 32% in native cyt *c* to 30% in the A-state (Goto et al., 1990a; Nishii et al., 1994). Finally, NMR-monitored H/D exchange experiments on the A-state revealed protection of amide protons in the N-terminal, C-terminal, and 60s helical regions but loss of structure for the short 50s and 70s helices (Jeng et al., 1990; Jeng & Englander, 1991).

The studies reported in this paper extend the structural characterization of A-state cyt *c* using resonance Raman (RR) spectroscopy. RR spectra show intensity enhancement of chromophore vibrational modes when the laser wavelength is tuned to an absorption band. Use of 200 nm excitation permits observation of peptide backbone vibrations, whose frequencies and intensities reveal details of protein secondary structure (Carey, 1982; Tu, 1982; Wang et al., 1991). With 230 nm laser radiation the vibrations of the aromatic amino acids tyrosine (Tyr) and tryptophan (Trp) are selectively observed, which are useful for probing tertiary structure changes through side-chain hydrogen bonding (Harada & Takeuchi, 1986; Austin et al., 1993a). Finally, laser excitation at 406.7 nm, resonant with the heme Soret absorption, enhances vibrational modes of the porphyrin macrocycle, which provide information on core-size, spin-state, and planarity (Spiro, 1983, 1985; Cartling, 1988; Spiro & Li, 1988). Spectra for the A-state are compared with those for the native protein and the acid-denatured state. The U-state has been shown by spectroscopic measurements to possess reduced CD ellipticity at 222 nm (f_H = 5%), an expanded radius of gyration (R_g = 24.2 Å), and greatly reduced fluorescence quenching (Goto et al., 1990a, 1993; Jeng & Englander, 1991; Kataoka et al., 1993). Although adding guanidinium hydrochloride unfolds cyt *c* more fully (R_g = 32.4 Å) than does acid (Kataoka et al., 1993), UVRR spectra are precluded because of excessive absorption of the UV light by the denaturant.

Results

Secondary structure

Laser radiation at 200 nm is resonant with the red edge of the absorption band of the peptide bond, and the resultant UVRR spectra of proteins contain bands for the amide I, II, III, and S vibrational modes. Amide II and III are the out-of-phase and in-phase combinations of the CN stretching and NH in-plane bending displacements, respectively, whereas amide I is a localized CO stretching vibration (Krimm & Bandekar, 1986). Although some ambiguity still remains over the assignment of the amide S mode (Song et al., 1991), the most likely candidate is a $C_\alpha H$ deformation vibration (Wang et al., 1991; Jordan & Spiro, 1994). These vibrational bands are useful probes of protein secondary structure. The amide I and III wavenumber values are sensitive to proportions of α-helix, β-sheet, and unordered structure in the protein (Carey, 1982; Tu, 1982), whereas the amide II and S intensities both exhibit a negative linear correlation with increasing helical content (Wang et al., 1991).

Figure 1 shows the 200-nm-excited UVRR spectra of N- and A-state cyt *c*, together with a difference spectrum that reveals small changes in band position and intensity. The A–N difference spectrum shows a derivative feature for the amide III region, with a negative component at 1,279 cm^{-1} and a positive component at 1,253 cm^{-1}. Amide III occurs in the range ca. 1,260–1,300 cm^{-1} for α-helices and ca. 1,240–1,250 cm^{-1} for random coil (Tu, 1982), and the difference spectrum therefore indicates a reduction in helical structure for the A-state and a concomitant increase in disordered polypeptide. A decrease in helicity is also supported by the increase of amide II intensity at 1,540 cm^{-1} upon conversion of cyt *c* to the A-state. Similar but more pronounced changes in amide III position and amide II intensity were also observed in a 200-nm UVRR study of acid- and alkali-denatured cyt *c* (Copeland & Spiro, 1985). No changes are detectable for the amide I and S modes upon forming the A-state because the amide I wavenumber value shows less variation than does amide I and because the small peak height of amide S renders intensity changes difficult to observe.

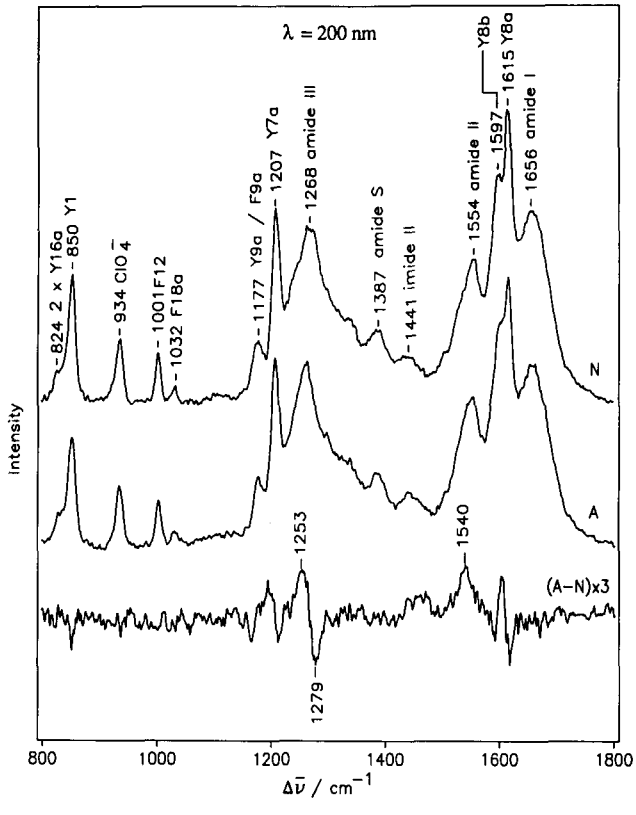

Fig. 1. The 200-nm UVRR spectra of N- and A-state cytochrome *c* showing enhancement of amide vibrational modes. N- and A-state samples are 1 mg/mL of protein with 1.5 M NaCl at pH 6.5 and 2.2, respectively. As an internal intensity standard, 0.15 M $NaClO_4$ was added. Spectra were collected from a flowing sample using 0.2 mW of laser power and are the sum of three 10-min scans. The difference spectrum (A–N) was generated using the ClO_4^- intensity standard at 934 cm^{-1}.

A previously established correlation between amide II peak height and helical content can be used to quantify the helical change (Wang et al., 1991). The N- and A-state UVRR spectra were fit to a sum of Lorentzian components to determine the band intensities, and the helical content was calculated from the peak height molar scattering ratio relative to the ClO_4^- internal standard. The height ratio $R = 30.0$ for N-state cyt *c* corresponds to a helical content of 37 ± 3%, which is comparable to the 45% helical content as determined by X-ray crystallography. The discrepancy likely arises from partial disordering for helical structures in solution as compared to the crystalline environment. NMR studies of NOE connectivities and H/D exchange for cyt *c* has shown that the C-terminal helicity is similar to the crystallographic structure, but that the peptide NH atoms of Lys 7 to Phe 10 in the N-terminal helix exhibit exchange behavior typical of dynamic fraying (Wand & Englander, 1986; Wand et al., 1986). The amide II height ratio in the UVRR spectrum increases to $R = 32.9$ upon formation of the A-state, corresponding to a helical content of 27 ± 3%. The increase in amide II intensity therefore indicates a decrease in helical content of 10 ± 5% upon formation of the A-state. A 200-nm UVRR spectrum for the U-state was not obtained because the absence of salt precludes the use of ClO_4^- as an internal intensity standard for quantitation of the helical content.

Cyt *c* contains five helical regions (Bushnell et al., 1990): three long helices, at the N-terminal (residues 6–14), C-terminal (87–102), and 60s region (60–69) of the sequence, plus two short helices in the 50s region (49–54) and 70s region (70–74). Previous measurements of the CD ellipticity at 222 nm ($[\theta]_{222}$) obtained a fractional helicity of 32% for native cyt *c*, with only a 2% decrease upon forming the A-state (Goto et al., 1990a; Nishii et al., 1994). However, quantitation of helical structure using far-UV CD is complicated by interference from aromatic side chains and by an overlapping contribution to $[\theta]_{222}$ from random coil configurations, which is opposite in sign to the helical signal (Johnson, 1990). The A-state was also studied using NMR-monitored H/D exchange experiments to monitor the presence of secondary structure (Jeng et al., 1990). Amide protons in the N-terminal, C-terminal, and 60s helices were still significantly protected in the A-state, although at a reduced level, whereas the 50s and 70s helices showed negligible protection. The two unprotected helical regions each contain six residues, and their combined contribution to the helical content is 11.5%. However because the protection factors obtained from these experiments depend on the kinetics for local unfolding and refolding (Englander & Mayne, 1992), it is possible to have regions of secondary structure that are insufficiently stable to be protected against exchange, but which can transiently contribute to a signal in optical spectroscopy (Elove et al., 1991). The ca. 10% helical reduction detected by UVRR spectroscopy therefore extends the NMR result by showing that the 50s and 70s helices are unfolded in the A-state rather than partially destabilized. It is unlikely that the change in helical content arises from additional dynamic fraying of the N- and C-terminal helices because the NMR experiments of Jeng et al. (1990) show H/D exchange protection for the same amide protons in these helices for both the N- and A-state structures.

Tertiary structure

Laser excitation at 230 nm produces enhancement of Trp and Tyr vibrational modes while minimizing the intensity from Phe (Fodor et al., 1989). The frequencies and intensities of Trp and Tyr bands contain information about protein tertiary structure because they are sensitive to side-chain conformation, hydrogen bonding, and environmental polarity (Harada & Takeuchi, 1986; Austin et al., 1993a). We have combined spectroscopic studies of cyt *c* with a molecular modeling analysis of side-chain hydrogen bonding, which has previously proved successful for interpreting the UVRR spectra of structural changes in hemoglobin (Rodgers et al., 1992) and fluoromethemoglobin (Jayaraman et al., 1993). Using the X-ray structural coordinates (Bushnell et al., 1990), hydrogen atoms were added to N_1 of the single Trp side chain (Trp 59) and to the O atoms of all Tyr side chains (Tyr 48, 67, 74, and 97). For Tyr side chains the C-O-H angle was fixed at 109.5°, but the C-OH torsional angle with respect to the plane of the ring was varied to minimize the distance between the hydrogen atom and the hydrogen bond acceptor. Hydrogen bond partners and geometries are listed in Table 1, together with torsional angles for all tyrosines. All of the geometric parameters are consistent with observed ranges for side-chain hydrogen bonding (Baker & Hubbard, 1984; Ippolito et al., 1990).

Table 1. *Hydrogen bonding geometries for tryptophan and tyrosine side chains in the X-ray crystal structure of oxidized horse heart cytochrome c*[a]

Side chain	H-bond partner	D-H···A dist. (Å)	D-H···A angle (°)	C-OH dihedral (°)[b]
Trp 59	Propionate O, ring A	1.76	158	–
Tyr 48	Propionate O, ring A	1.40	152	37
Tyr 67	Met 80, S	2.44	142	22
Tyr 74	H_2O[c]	1.45	164	3
Tyr 97	None	–	–	–[d]

[a] Hydrogen atoms were added to Trp and Tyr side chains using the X-ray crystallographic coordinates of Bushnell et al. (1990) as described in the Materials and methods.

[b] Dihedral angle of the (O)H atom with respect to the tyrosine plane, given in the range $0 < \tau < 90°$.

[c] Crystallographically located water molecule 139H, located near the solvent-exposed surface.

[d] The Tyr 97 side chain has no hydrogen bonding partner that could be detected by molecular modeling and the COH dihedral angle therefore cannot be determined.

The 230-nm UVRR spectra of the N-, A-, and U-states of cyt *c* are shown in Figure 2. Strong enhancement of Trp fundamental modes for native cyt *c* are observed for W3 (1,556 cm^{-1}), W5 (1,458 cm^{-1}), W7 (1,351 cm^{-1}), W10 (1,236 cm^{-1}), W16 (1,014 cm^{-1}), and W17 (878 cm^{-1}), together with the 2 × W18 overtone (1,510 cm^{-1}) (Austin et al., 1993a). A large intensity decrease is observed for these bands upon conversion of cyt *c* to the A-state, which results from a change in environment for the single Trp 59 side chain. The variation of RR intensity with incident wavelength can be quantified by measurement of Raman excitation profiles (REPs). The REPs for the W18, W16, and W3 bands of Trp 59 in native cyt *c* are significantly red-shifted compared to aqueous Trp, resulting in a large scattering cross section for laser excitation at 230 nm (Liu et al., 1989). This effect can be attributed to the hydrophobic environment of the Trp 59 side chain and its strong hydrogen bond to the propionate group on ring A of the heme (Table 1). For comparison, the W3 REP for 3-methylindole, a tryptophan model compound, was most red-shifted in cyclohexanol, a solvent that provides a fairly nonpolar environment plus the ability to accept an N_1H hydrogen bond (Rodgers et al., 1992). The decrease in Trp mode intensity for the A-state reflects a ca. 5-nm blue shift in the Trp 59 resonance enhancement maximum, as judged from the REPs (Liu et al., 1989). This change would be expected to accompany a decrease in hydrophobicity of the Trp 59 side-chain environment and/or breaking of the side-chain hydrogen bond.

Information about the Trp 59 side-chain environment can also be obtained from the Fermi resonance doublet at ca. 1,340/1,360 cm^{-1}, which arises from interaction between W7 and one or more out-of-plane modes (Harada et al., 1986; Austin et al., 1993a). The W7 band profiles for N-, A-, and U-state cyt *c* are given in Figure 3, together with their curve fits and resolved components. The W7 region for N-state cyt *c* is unusual among UVRR spectra of proteins because instead of a doublet there exists a broad unresolved band centered at ca. 1,350 cm^{-1} that requires three components for an accurate fit. However, Harada et al. (1986) also observed three components for the W7 region using nonresonant Raman spectroscopy, which they attributed to Fermi resonance between W7 and two out-of-plane combination bands (930 + 423 cm^{-1} and 743 + 608 cm^{-1}). Strong enhancement of the 1,349.7-cm^{-1} band in the UVRR spectrum of native cyt *c* may arise from the unusually strong hydrogen bond for the Trp 59 side chain. Conversion of cyt *c* to the A-state results in a W7 band that shows a more typical doublet profile, with an approximately 1:2 ratio between the 1,339.8- and 1,356.6-cm^{-1} components. The observed W7 band shape for A-state cyt *c* is similar to that for myoglobin where the Trp side chains are buried in a partially hydrophobic environment (Austin et al., 1993a). Miura et al. (1988) have also shown that the ca. 1,360-cm^{-1} component increases with respect to the ca. 1,340-cm^{-1} component upon increasing environmental hydrophobicity of the Trp side chain. The W7 band profile for the

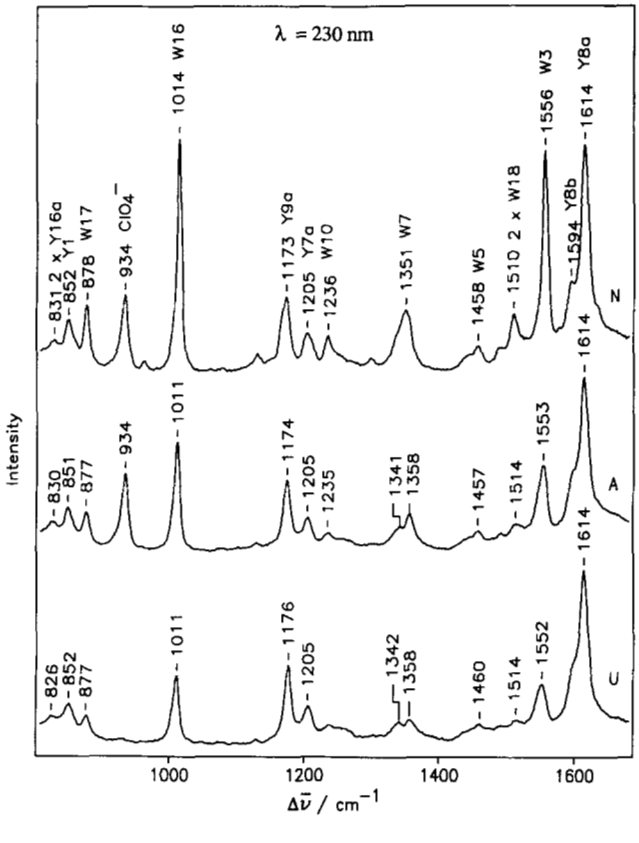

Fig. 2. The 230-nm UVRR spectra of N-, A-, and U-state cyt *c* showing enhancement of Tyr and Trp vibrational modes. N- and A-state samples are 2 mg/mL of protein with 1.5 M NaCl and 0.15 M $NaClO_4$ at pH 6.5 and 2.2, respectively. The U-state sample was 2 mg/mL of protein at pH 2.0 in the absence of salt. Spectra were obtained from a flowing sample using 0.3 mW of laser power and are the sum of three 10-min accumulations.

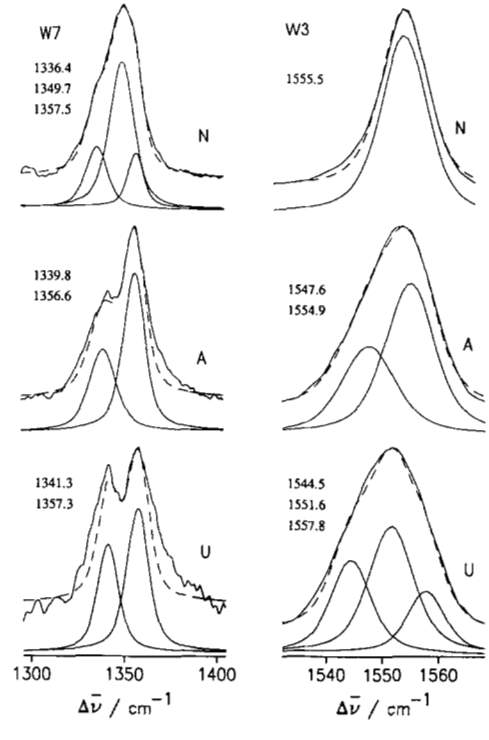

Fig. 3. Band shapes (solid lines) and curve fits (dashed lines) for the W7 and W3 bands of the N-, A-, and U-state. The component bands, whose peak positions are given in the figure, were determined by curve fitting the spectra to a minimal number of 50% Lorentzian/Gaussian functions while restricting the variation in bandwidth.

A-state therefore suggests that the Trp 59 side chain remains in the hydrophobic heme pocket through partial preservation of tertiary structure in this region. In the U-state, however, the W7 profile is identical to that for aqueous Trp, with almost equally intense components, showing that the Trp 59 side chain has become exposed to the solvent water. This observation agrees with a large increase in the fluorescence quantum yield for the U-state, which indicates that Trp 59 no longer resides in the heme pocket (Jeng & Englander 1991).

The wavenumber position of certain Trp bands can provide further information about the Trp 59 side-chain environment. Studies of the W3 mode, which is mostly a C_2-C_3 (pyrrole) stretching vibration, have revealed only a weak correlation of frequency with solvent hydrogen bonding (Miura et al., 1989; Rodgers et al., 1992). However, the W3 band position exhibits a dependence on the magnitude of the C_2-C_3-C_β-C_α angle, designated $|\chi^{2,1}|$, as measured in several crystalline Trp derivatives, with a shift to higher frequency as the $|\chi^{2,1}|$ angle increases (Miura et al., 1989). Figure 3 shows the W3 band shapes, curve fits, and components for the N-, A-, and U-states of cyt *c*. The high frequency (1,555.5 cm^{-1}) for W3 in N-state cyt *c* indicates a $|\chi^{2,1}|$ angle for the Trp 59 side chain that is greater than 120°, but the correlation levels off at larger angles. The $|\chi^{2,1}|$ value measured for Trp 59 in the crystal structure is 144°, which is consistent with the W3 band position. The W3 band shape is narrow and symmetric, indicating that the Trp 59 side chain adopts a single conformation. In the A-state, by contrast, the W3 band is broad and asymmetric, suggesting a heterogeneous population of rotamers. The A-state band shape can be fit to two components, with a major band at 1,554.9 cm^{-1} and a shoulder at 1,547.6 cm^{-1}. This result suggests that the majority rotamer population remains in a similar orientation as the native protein, whereas the minority population exhibits a $|\chi^{2,1}|$ angle close to 90° as calculated using the correlation of Miura et al. (1989). Interestingly, a survey of protein crystal structures by Ponder and Richards (1987) has found that the $|\chi^{2,1}|$ dihedral angles for Trp side chains are clustered around 90°, suggesting a possible energetic minimum for this conformation. The curve fit for W3 in the U-state requires three components at 1,544.5, 1,551.6, and 1,557.8 cm^{-1}, reflecting a range of $\chi^{2,1}$ angles that varies from below 60° to above 120°. This broad range of angles is consistent with loss of tertiary structure in the U-state.

The W17 vibration of the Trp side chain contains a significant contribution from the N_1H in-plane bending displacement and was investigated as a structural marker for indole hydrogen bonding. Miura et al. (1988) studied a series of crystalline tryptophan analogs and showed a linear correlation between W17 and the N–H stretching frequency, where the position of W17 downshifts with increasing hydrogen bond donation. We sought to use this correlation to interpret changes in the W17 band for N-, A-, and U-state cyt *c*, which are shown in Figure 4. The strong side-chain H-bond for Trp 59 in native cyt *c* would be expected to lower the W17 band to ca. 870 cm^{-1}. W17 is instead observed at 878.4 cm^{-1}, a position that correlates with moderate to weak hydrogen bonding. In the A-state the peak downshifts by 0.6 cm^{-1}, but shifts back again to 878.5 cm^{-1} for the unfolded protein. It is difficult to rationalize these results in terms of Trp 59 hydrogen bonding in different cyt *c* folding states. UVRR studies of hemoglobin also reveal no changes in W17 position upon switching between R and T quaternary states, even though the hydrogen bonding partner for the interfacial Trp β37 side chain changes from the backbone carbonyl of Asn β102 to the side-chain carboxylate of Asp α94 (Rodgers et al., 1992; Jayaraman et al., 1993). Therefore the W17 behavior observed by Miura et al. (1988) for Trp model compounds should be viewed with caution when interpreting the UVRR spectra of proteins.

We also investigated the intense tryptophan mode W18, an indole ring breathing vibration, as a possible structural marker band. The W18 bands and curve fits for N-, A-, and U-state cyt *c* are shown in Figure 4. The higher frequency component, which is currently unassigned, remains approximately fixed at ca. 765 cm^{-1}, and appears to increase in relative intensity for the A- and U-state spectra because the Trp band intensity is decreasing. The W18 band shifts up by 1.6 cm^{-1} upon conversion of cyt *c* from the native protein to the A-state, which is consistent with the ca. 3.5-cm^{-1} upshift observed for the W18 overtone. The W18 position shows little additional change in the U-state UVRR spectrum. The W18 vibrational mode itself has not been extensively studied because its position at ca. 760 cm^{-1} falls outside the standard spectral window for diode array detection (800–1,700 cm^{-1}), although the 2 × W18 overtone is commonly observed at ca. 1,510 cm^{-1}. No frequency shift for 2 × W18 was observed in the 230-nm UVRR difference spectrum (T–R) of hemoglobin (Rodgers et al., 1992) and fluoromethemoglobin (Jayaraman et al., 1993), although a small intensity increase occurred in both cases. Recently, Cho et al. (1994) have directly monitored the W18 mode for the quaternary transition in fluoromethemoglobin using 229 nm excitation. They confirm the absence of a frequency shift, and in addition report a very

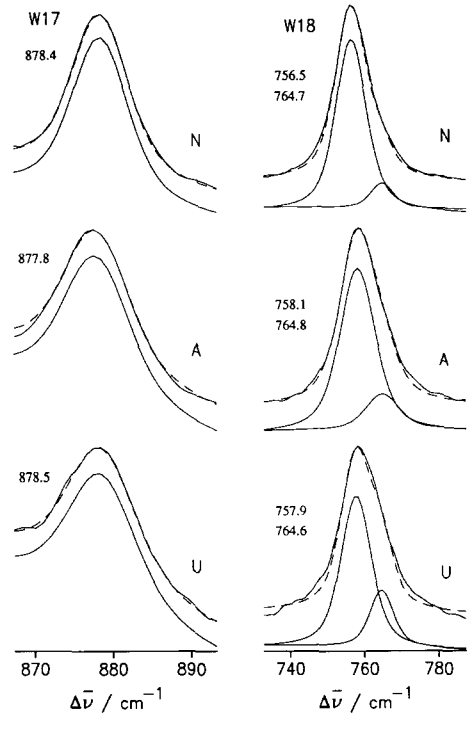

Fig. 4. Band shapes (solid lines), curve fits (dashed lines), and components for the W17 and W18 bands of the N-, A-, and U-state. Components were obtained as described in the legend to Figure 3.

large intensity increase for the mode fundamental at 759 cm^{-1}. Although it is not possible at present to correlate this behavior with specific structural properties of the protein, future studies of the frequency and intensity of W18 may reveal this mode to be a sensitive indicator of the Trp side-chain environment.

Laser excitation at 230 nm also produces enhancement of the Tyr vibrational modes Y8a (1,614 cm^{-1}), Y8b (1,594 cm^{-1}), Y7a (1,205 cm^{-1}), Y9a (1,173 cm^{-1}), and the Fermi doublet interaction between Y1 and 2xY16a (852 and 831 cm^{-1}) (Austin et al., 1993a). In contrast to Trp bands, which can be uniquely assigned to the Trp 59 side chain, the Tyr bands contain contributions from the four side chains Tyr 48, 67, 74, and 97. The hydrogen bonding geometries for these side chains are listed in Table 1. Tyr 48 donates a strong hydrogen bond to the propionate group on ring A of the heme, which is buried in the hydrophobic core. Tyr 67 donates a hydrogen bond to the sulfur atom of the Met 80 side chain, and accepts a hydrogen bond from a localized water molecule (Wat 112) that is conserved in all eukaryotic cyt *c* proteins (Bushnell et al., 1990; Berghuis et al., 1994a). The hydrogen bonding network around Tyr 67 is conformationally important because mutation of this side chain to Phe in the homologous yeast cyt *c* protein causes substantial changes of the heme pocket structure (Berghuis et al., 1994b). The side chain of Tyr 74 forms a hydrogen bond with a water molecule near the solvent-accessible surface, whereas Tyr 97, also located at the surface, has no detectable hydrogen bonding partner.

Changes in hydrogen bonding are revealed by intensities and frequencies of Tyr bands in the UVRR spectra. The REPs of the vibronically active modes Y8a, Y9b, and Y9a are red-shifted upon phenolic hydrogen bond donation (Fodor et al., 1989) and their intensity reduction in the A-state spectrum is indicative of reduced side-chain hydrogen bonding. The position of the Y8b mode, assigned to a C–C stretching vibration, decreases in frequency upon increased phenolic hydrogen bond donation (Rodgers et al., 1992). Because the Y8a and Y8b bands significantly overlap, the region was curve fit to a sum of component bands as shown in Figure 5. The Y8a/Y8b region for native cyt *c* required three components for an accurate fit, especially in the region between the peak maxima, whereas for the A- and U-states the additional peak caused only slight improvement and was not included. The Y8b components for the N-state arise from two structural classes of Tyr side chain. The majority Y8b component at 1,593.1 cm^{-1} (full width at half maximum [FWHM] = 10.4 cm^{-1}) corresponds to very strong hydrogen bond donation, with an enthalpy of ca. 6 kcal/mol as measured using *p*-cresol (Rodgers et al., 1992). In view of the structural data (Table 1), we assign the Tyr 48 side-chain to this band. The side-chain hydrogen bonding of Tyr 67 and 74 is weaker but still favorable, so we infer that they also contribute to the majority component. The position of the minority Y8b component at 1,601.3 cm^{-1} (FWHM = 9.1 cm^{-1}) suggests an absence of hydrogen bonding, and we assign this component to the Tyr 97 side chain, which possesses no hydrogen bonding partner. In the A-state UVRR spectrum the Y8b band broadens (FWHM = 13.1 cm^{-1}) and upshifts by 3.5 cm^{-1} to 1,596.6 cm^{-1}. This change in Y8b position indicates that the net phenolic hydrogen bonding enthalpy is reduced by ca. 4.5 kcal/mol (Rodgers et al., 1992) and can be ascribed to disruption of tertiary structure for the Tyr 48, 67, and 74 side chains. Tyr 48 is located at the N-terminus and Tyr 74 at the C-terminus of the 50s and 70s helices, respectively, which both unfold in the A-state. Although Tyr 48 is located in the structurally preserved 60s helix, the native Met 80 ligand, which accepts its hydrogen bond, is displaced in the A-state (see below). In the U-state the Y8b component upshifts by an additional 0.5 cm^{-1} with a slight increase in width (FWHM = 13.4 cm^{-1}), suggesting only small additional changes in tertiary structure.

Changes in Tyr side-chain hydrogen bonding can also be used to interpret the behavior of the Y9a mode at ca. 1,175 cm^{-1}, where the pronounced band shape heterogeneity for native cyt *c* is lost in the A- and U-state spectra (Fig. 5). The Y9a vibration contains contributions from COH and CCH bending displacements (Harada & Takeuchi, 1986). In studies of *p*-cresol, Takeuchi et al. (1989) found no simple correlation of the Y9a mode position with phenolic hydrogen bonding. They did suggest, however, that the Y9a frequency could depend on the C-OH dihedral angle with respect to the ring plane. When the phenolic hydrogen atom is coplanar with the aromatic ring, steric repulsion with the ring hydrogen atoms will provide a small additional restoring force that will increase the frequency of the COH bending vibration; this interaction will be removed when the phenolic hydrogen moves out of the ring plane, with a concomitant lowering of the Y9a frequency. We used molecular modeling to investigate the orientation of the C-OH dihedral angle ($0 < \tau < 90°$) for the three hydrogen bonded tyrosines in the native protein, and the results are listed in Table 1. The τ angles of 37° for Tyr 48, 22° for Tyr 67, and 3° for Tyr 74 can be correlated with Y9a components at 1,167.2, 1,173.1, and 1,177.7 cm^{-1}, respectively. The broader component at 1,167.2 cm^{-1} may also encompass the C-OH dihedral angle for Tyr 97; because the phe-

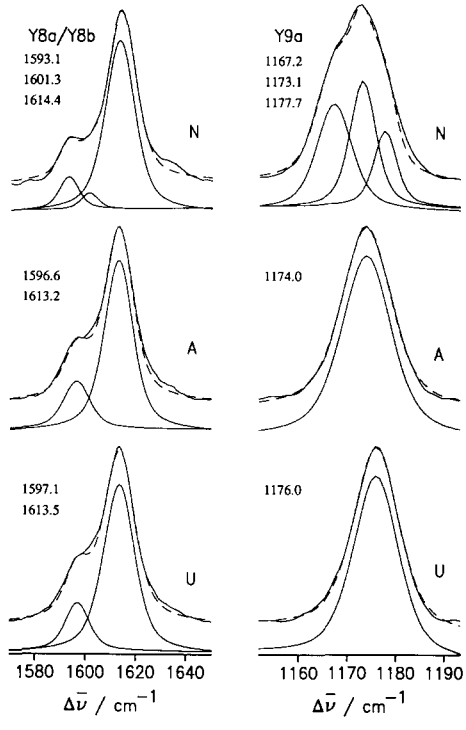

Fig. 5. Band shapes (solid lines), curve fits (dashed lines), and components for the Y8a/Y8b and Y9a bands of the N-, A-, and U-state. Components were obtained as described in the legend to Figure 3.

nolic hydrogen of this side chain is unconstrained by hydrogen bonding, it may exhibit a nonplanar orientation of the phenolic hydrogen atom to minimize steric repulsion with the ring hydrogens. The observed properties of Tyr 67 and Tyr 74 agree well with those reported by Takeuchi et al. (1989) for crystals of L-tyrosine ethyl ester ($\tau = 17.4°$, $\nu_{9a} = 1{,}173\ cm^{-1}$) and L-tyrosine hydrochloride ($\tau = 1.4°$, $\nu_{9a} = 1{,}177\ cm^{-1}$), but no data were available for crystalline tyrosine derivatives with larger τ angles. In the A-state spectrum the Y9a mode collapses to a symmetric band at 1,174.0, indicating loss of tertiary hydrogen bonding, and remains similarly unstructured in the U-state spectrum.

Heme ligation and structure

The heme macrocycle, shown in Figure 6, is covalently bonded to the protein through thioether links to Cys 14 and Cys 17, with two axial ligands provided by the side chains of His 18 and Met 80. One propionate group, on pyrrole ring A of the heme, is buried in the hydrophobic core, accepting hydrogen bonds from the side chains of Arg 38, Tyr 48, Asn 52, and Trp 59. The second propionate, on pyrrole ring D, extends to the solvent-accessible surface and is hydrogen bonded to Thr 49 and Thr 78.

The spin state of the heme iron in cyt *c*, which is determined by the number and type of axial ligands, can be probed by UV/visible absorption and RR spectroscopy. In low-spin d^5 Fe(III) porphyrins ($S = 1/2$) the electrons reside in the nonbonding d_{xy} and d_π (d_{xz},d_{yz}) orbitals. Transfer of electrons to the antibonding d_z2 and $d_x2\text{-}_y2$ orbitals produces a high-spin heme ($S = 5/2$), resulting in a blue shift of the Soret absorption and the possibility of porphyrin-to-iron charge transfer bands (Makinen & Churg, 1983). The absorption spectra for the N-, A- and U-states are shown in Figure 7, where the 300–600-nm region contains the intense Soret band and weaker Q-bands and the 600–800-nm region contains the much weaker charge transfer absorptions (Makinen & Churg, 1983). Population of the $d_x2\text{-}_y2$ orbital in high-spin iron results in expansion of the porphyrin core, defined as the average distance between the pyrrole nitrogen atoms and the central metal, which in turn causes downshifts in frequency for several skeletal vibrational modes (Spiro & Li, 1988). The most useful spin-state marker bands are ν_2, which is primarily a $C_\beta C_\beta$ stretching vibration, and ν_3 which contains similar contributions from $C_\beta C_\beta$ and $C_\alpha C_m$ stretching. The $C_\alpha C_m$ stretching vibration ν_{10} is also sensitive to core size, but its weak intensity in RR spectra for the A- and U-state limit its diagnostic usefulness. The RR spectra for the cyt *c* folding states are shown in Figures 8 and 9.

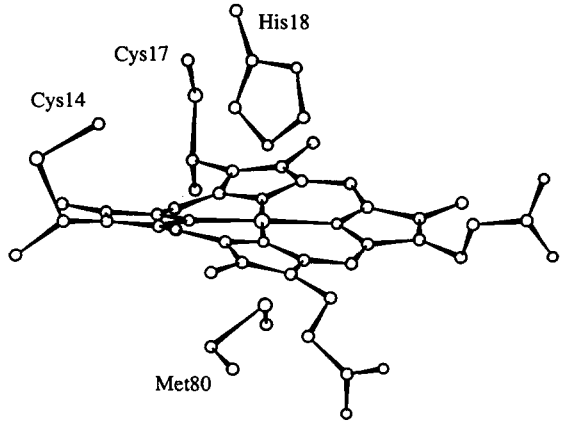

Fig. 6. Structure and ligation of the heme in horse heart cyt *c* (Bushnell et al., 1990). The heme is covalently linked to the polypeptide chain via thioether links to Cys 14 and Cys 17, with axial ligation to the heme iron atom provided by the side chains of His 18 and Met 80.

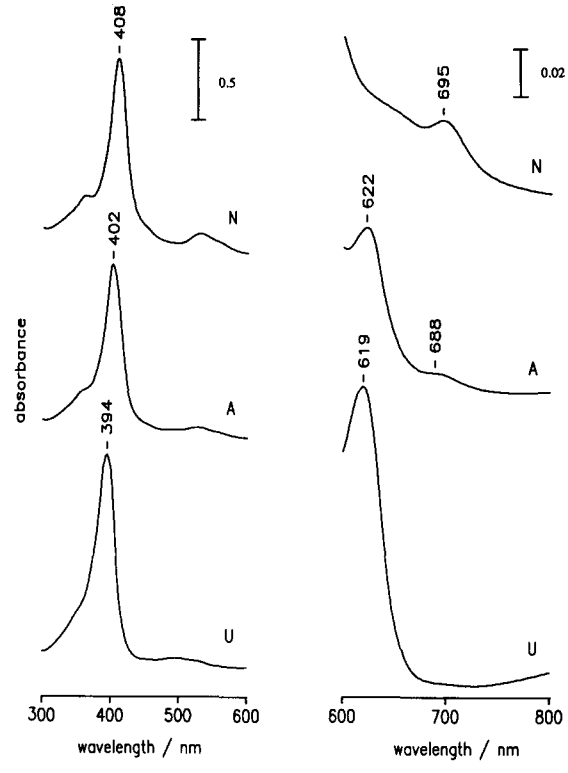

Fig. 7. UV/visible absorption spectra for the folding states of cyt *c*. Samples were prepared as described in the legend to Figure 2. Spectra were obtained using a quartz cell with a pathlength of 1 mm (300–600-nm region) or 10 mm (600–800-nm region).

Native cyt *c* shows a heme Soret maximum at 408 nm, which is typical for a low-spin heme iron atom, arising from axial coordination to the strong field ligands His 18 and Met 80. The weak absorption at 695 nm, which is polarized perpendicular to the heme plane, is diagnostic for Met 80 coordination to the heme iron (Makinen & Churg, 1983). The presence of a six-coordinate low-spin heme iron is confirmed in the RR spectrum by the positions of ν_2 (1,585 cm^{-1}), ν_3 (1,502 cm^{-1}), and ν_{10} (1,635 cm^{-1}). The ν_4 mode, consisting of $C_\alpha N$ and $C_\alpha C_\beta$ bond stretches, is primarily sensitive to iron oxidation state, and its position at 1,373 cm^{-1} is typical for an Fe(III) atom (Cartling, 1988).

In the A-state the Soret absorption maximum shifts to 402 nm, a position intermediate between the values for low- and high-spin hemes. This maximum could arise either from an intermediate spin heme ($S = 3/2$) or an equilibrium mixture of high- and low-spin species. The 695-nm absorption disappears, indicating loss of Met 80 ligation to the heme iron atom. The 622-nm and 688-nm bands, which are observed only for high-spin iron porphyrins, arise from charge transfer absorption from the porphyrin a_{2u} orbital to the iron d_π orbitals and d_z2 orbital, respec-

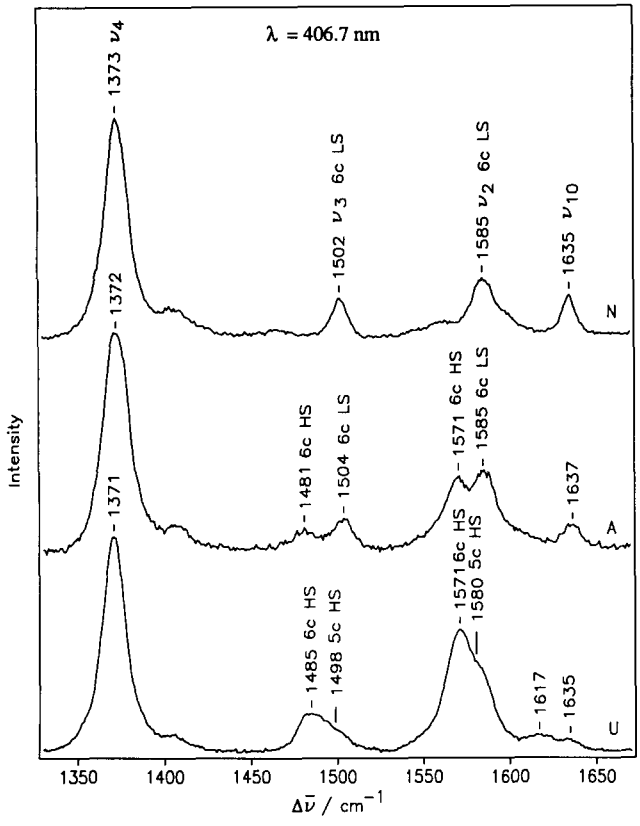

Fig. 8. High-wavenumber region and band assignments for 406.7-nm RR spectra of the N-, A-, and U-states of cyt *c*. Samples were prepared as described in the legend to Figure 2. Spectra were obtained with 30 mW of 406.7-nm laser radiation and collected at 4-cm^{-1} resolution with a scan rate of 2 s per wavenumber. Data shown are the sum of three scans. The figure gives mode assignments and the presence of low-spin (LS), high-spin (HS), five-coordinate (5c), and four-coordinate (4c) species.

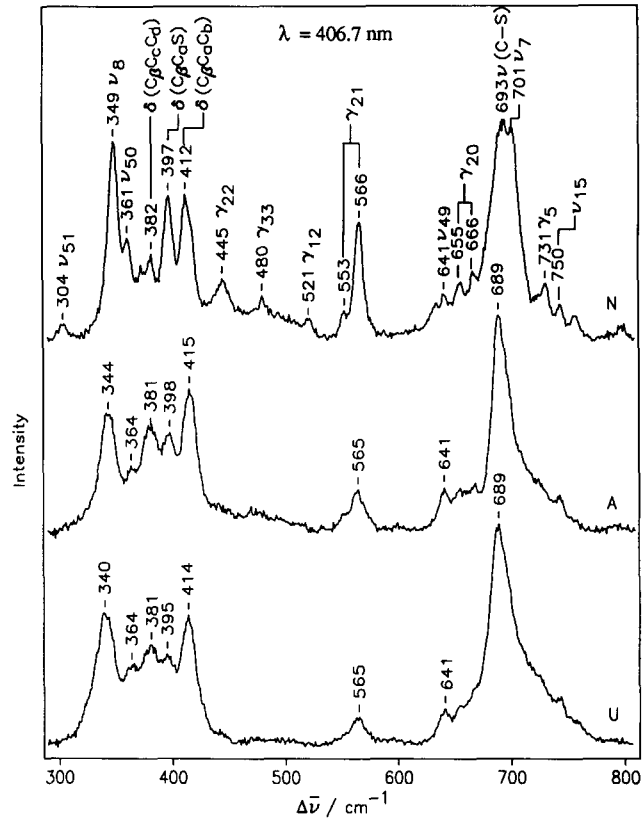

Fig. 9. Low-wavenumber region and band assignments for 406.7-nm RR spectra of the N-, A-, and U-states of cyt *c*. Spectral acquisition is described in the legend to Figure 7.

tively (Makinen & Churg, 1983). Similar charge transfer bands have been observed in the absorption spectrum of aquometmyoglobin (Makinen & Churg, 1983). Further support for His 18/H_2O coordination in the A-state is provided by a recent study of a cyt *c* mutant in which the native Met 80 ligand is replaced by alanine, thereby permitting an exogenous ligand to occupy an axial binding site (Bren & Gray, 1993). At pH 4.5, when a water molecule is coordinated to the heme, the absorption spectrum closely resembles that of the A-state, with a Soret maximum at 400 nm and a charge transfer band at 620 nm.

In the A-state RR spectrum the ν_4 mode shows little change, consistent with preservation of an Fe(III) heme. The most noticeable spectral difference is the presence of two bands for the spin-state marker bands ν_2 (1,571 and 1,585 cm^{-1}) and ν_3 (1,481 and 1,504 cm^{-1}). These doublets confirm the presence of a mixed spin heme iron because the two components are each typical for six-coordinate low-spin and high-spin species. Similar mixtures of high- and low-spin states, detected as doublets for ν_2 and ν_3, have been observed for aquo-methemoglobin (Kitagawa & Nagai, 1979), hydroxy-metmyoglobin (Strekas & Spiro, 1974; Asher & Schuster, 1979), and His 175/OH^- coordination in the Asp 235 Asn mutant of Fe(III) cyt *c* peroxidase (Smulevich, 1993). A spin-state mixture arises when placing electrons in the antibonding d_z2 and $d_x2\text{-}_y2$ orbitals is energetically comparable to the spin pairing energy in the bonding d_{xy} and $d_\pi(d_{xz},d_{yz})$ orbitals. The energy of the $d_x2\text{-}_y2$ orbital is determined primarily through interactions with the pyrrole nitrogen atoms and is relatively insensitive to axial ligation. Axial binding of an H_2O molecule, a weak π-donor ligand, raises the energy of the iron d_π orbitals to a position close to the d_z2 orbital, and promotion of electrons from d_π to the antibonding orbitals then becomes energetically favorable. The complete absence of absorption intensity at 695 nm for the A-state argues against an alternative interpretation of the absorption and RR data in which the low-spin component arises from a conformational population with residual Met 80 coordination.

The U-state absorption spectrum shows a Soret maximum at 394 nm, which is characteristic for a high-spin heme. Goto et al. (1993) have shown that the Soret position reflects unfolding of the polypeptide chain, as detected by reduced quenching of Trp 59 fluorescence and loss of CD ellipticity at 222 nm. There is a small blue shift and strong intensity increase for the a_{2u}–d_π charge transfer absorption, suggesting higher energy d_π orbitals and an increased high-spin component compared to the A-state. Disappearance of the 688-nm band for the U-state would be expected from a lowering of the d_z2 orbital energy upon loss of axial ligation. The RR spectra for the U-state show unresolved doublets for the ν_2 and ν_3 bands, which agrees with a previous study by Myer and Saturno (1991). The frequencies indicate a major component arising from six-coordinate high-spin

heme and a minor contribution from a five-coordinate high-spin species (Smulevich, 1993). The axial ligand in the five-coordinate heme is probably a single H_2O molecule, whereas the sixth ligand could be another H_2O or His 18 with a weakened axial bond (Dyson & Beattie, 1982).

Whereas the high-wavenumber region (1,300–1,700 cm^{-1}) of the heme RR spectrum provides information on spin state for the central iron atom, the low-wavenumber region (300–800 cm^{-1}) contains structural information on the porphyrin macrocycle. This spectral region is unusually complex (Cartling, 1988), but reconstitution of isotopically labeled hemes into yeast-iso-cyt *c* has recently permitted the assignment of almost all low-wavenumber vibrational bands (Hu et al., 1993). In the spectrum of native cyt *c* there is strong enhancement of two modes assigned to vibrations of the thioether linkages, specifically $\delta(C_\beta C_a S)$ at 397 cm^{-1} and ν(C–S) at 693 cm^{-1}. These modes both show a substantial intensity decrease in the A-state RR spectrum, although the ν(C–S) band becomes overlapped with the downshifted ν_7 vibration. These changes probably arise through alteration of the thioether linkage geometry in the A-state protein structure. Similar intensity changes for the thioether bands have been observed in the RR spectrum of a cyt *c* mutant in which Met 80 has been replaced by cysteine, causing structural reorganization of the heme pocket (Smulevich et al., 1994).

One surprising feature in the low-wavenumber RR spectrum of native cyt *c* is the strong enhancement of out-of-plane modes, most noticeably γ_{21} (553 and 566 cm^{-1}), but also γ_{22} (445 cm^{-1}), γ_{33} (480 cm^{-1}), γ_{12} (521 cm^{-1}), γ_{20} (655 and 666 cm^{-1}), and γ_5 (731 cm^{-1}). Resonance enhancement of out-of-plane modes derives from a distortion of the porphyrin macrocycle from a planar D_{4h} geometry. As shown in Figure 6, the heme in native cyt *c* exhibits a pronounced propeller distortion, where the $C_\beta C_\beta$ bonds deviate by an average of 10.5° from the plane of the pyrrole nitrogen atoms (Bushnell et al., 1990). Vibrational modes of e_g symmetry in the D_{4h} point group, such as γ_{21}, have their degeneracy lifted by a ruffling distortion that lowers the symmetry of the heme. The degenerate mode then splits into a doublet in which one component is totally symmetric and therefore subject to resonance enhancement via an A-term mechanism. The modes γ_{20} and γ_{21} arise from symmetric and asymmetric pyrrole folding vibrations, respectively, whereas γ_{22} is assigned to a pyrrole swiveling mode (Li et al., 1991). All but one of the out-of-plane modes disappear in the A-state RR spectrum, and the intensity of the remaining γ_{21} mode is greatly reduced. This change is probably caused by relaxation of the heme toward a planar structure through decreased protein contacts. However, residual intensity for the γ_{21} mode suggests the presence of weak heme–protein contacts in the A-state structure. There is a small additional intensity reduction for γ_{21} upon formation of the U-state, indicating further relaxation of the heme toward planarity, but γ_{21} disappears only in RR spectra obtained under very harsh denaturing conditions (9 M urea, pH 3) when the polypeptide chain is completely unfolded (Kataoka et al., 1993). Changes in heme planarity between native and unfolded states have also been detected using Soret CD spectroscopy (Myer 1978; Myer & Pande, 1978).

Discussion

The results described above, in conjunction with previous experimental studies, enable us to propose a structural model for the A-state. The model is summarized in Figure 10, which, for illustrative purposes, employs the coordinates of native cyt *c* (Bushnell et al., 1990). The A-state structure consists of a folded protein subdomain containing the heme together with the N-terminal, C-terminal, and 60s helices. The critical role of the heme in stabilizing polypeptide structure in cyt *c* has been demonstrated by peptide models of the N- and C-terminal helices (Wu et al., 1993) and by several studies of polypeptide disorder

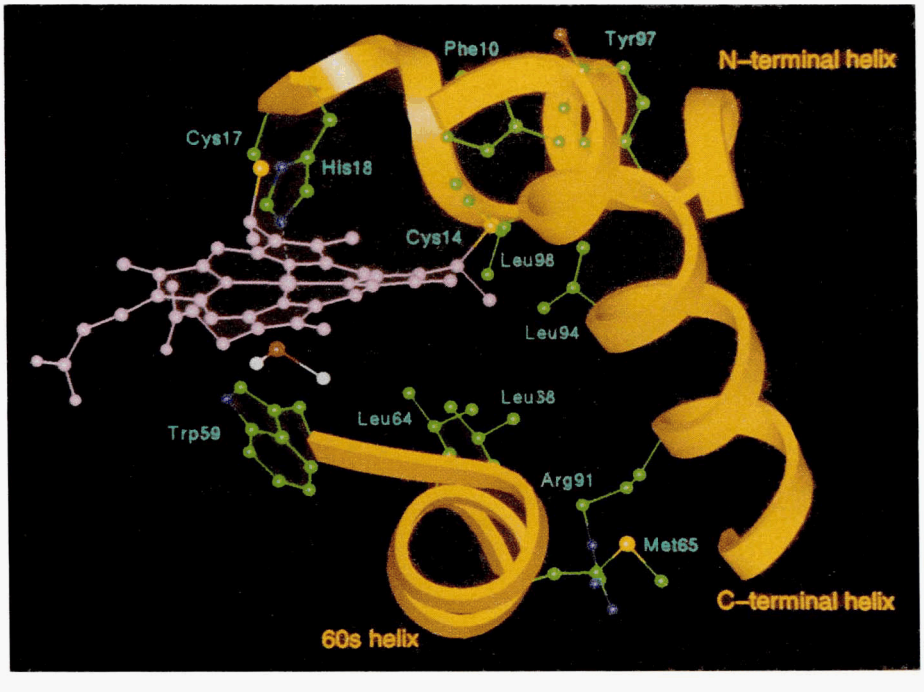

Fig. 10. Model for the A-state of cyt *c* using the X-ray crystallographic coordinates of the native protein (Bushnell et al., 1990). The A-state is a folded subdomain containing the N-terminal, C-terminal, and 60s helices and is stabilized by interhelical and heme–polypeptide interactions as described in the text. The heme iron is axially coordinated to His 18, but the native Met 80 ligand has been displaced by a water molecule. The Trp 59 side chain remains close to the heme but is conformationally disordered and the hydrogen bond to the heme propionate group is broken.

in apocytochrome *c* (Stellwagen et al., 1972; Fisher et al., 1973; Hamada et al., 1993; Dumont et al., 1994).

The 200-nm UVRR spectra reveal an ca. 10% decrease in helicity for the A-state, consistent with unfolding of the short 50s and 60s helices (Jeng et al., 1990). Inspection of the native state crystal structure reveals likely candidates for the interactions that stabilize the remaining N-terminal, C-terminal, and 60s helices in the A-state structure (Bushnell et al., 1990). The heme is anchored to the polypeptide at the N-terminal helix through thioether bonds to Cys 14 and Cys 17 and through axial coordination to His 18. This helix possesses no nonbonding heme contacts, but interacts with the C-terminal helix at the interface between Tyr 97 and Gly 6/Phe 10 (Fredericks & Pielak, 1993). The side chains of Leu 94 and Leu 98, located in the C-terminal helix, make Van der Waals contacts to the methyl group on pyrrole ring B of the heme. The 60s region of the sequence, which displays negligible helicity in isolation (Kuroda, 1993), can be stabilized in the A-state through side-chain contacts between Leu 64 and Leu 68 and heme pyrrole rings A and B, respectively. The 60s helix also interacts with the C-terminal helix because the side chain of Arg 91 makes Van der Waals contact with the Met 65 side chain while the N_ϵ atom of Lys 99 forms a salt bridge with the side chain of Glu 61 (not shown). Loss of structure for the 50s and 70s helices probably occurs because of the absence of side-chain contacts with the heme or other helical regions.

The tertiary structure of the A-state is less compact than for the native protein, as indicated by an increase in the radius of gyration from 13.5 Å to 17.4 Å (Kataoka et al., 1993). The tertiary position of Trp 59 is mostly retained in the A-state, as shown by the persistence of fluorescence quenching (Jeng & Englander, 1991) because it resides at the N-terminus of the structurally preserved 60s helix. However, Trp modes in the 230-nm UVRR spectrum show that the side-chain orientation is disordered and the hydrogen bond to the heme propionate is probably broken. The Tyr 48, 67, and 74 side chains lose their tertiary hydrogen bonds in the A-state, as revealed by the 3.5-cm^{-1} upshift of Y8b and the loss of band shape heterogeneity for Y9a. Tyr 48 and Tyr 74 are located at the termini of the unfolded 50s and 70s helices, respectively, whereas the Tyr 67 hydrogen bond is lost upon disruption of Met 80 ligation.

Heme coordination in the A-state can be obtained from UV/visible absorption and 406.7-nm RR spectroscopy. The absence of a 695-nm absorption band for the A-state indicates loss of the native Met 80 ligand, but the position of the Soret band at 402 nm does not distinguish between an intermediate spin versus a mixed-spin heme. However, the RR doublets observed for the spin-state marker bands ν_2 and ν_3 are diagnostic for mixed spin, which arises from axial coordination of His 18 and a water molecule. The His 18 side chain remains coordinated in the A-state, despite the low solution pH because it resides in the folded subdomain and is protected from solvent. Conversely, loss of secondary and tertiary structure near Met 80 permits its replacement by a water molecule at the solvent-exposed face of the heme. The geometry of the heme macrocycle can be monitored by out-of-plane vibrational modes (Hu et al., 1993), most notably γ_{21}, whose RR intensity is activated by the nonplanar distortion induced by packing against polypeptide chain. The reduced intensity for out-of-plane modes in the A-state RR spectrum suggests reduced heme–polypeptide contact, but the γ_{21} intensity remains larger than the value observed for the unfolded protein.

The structure of the A-state can also be compared with kinetic intermediates that have been studied by time-resolved fluorescence, absorption, CD, and NMR-monitored H/D exchange (Roder et al., 1988; Elove & Roder, 1991; Elove et al., 1991, 1994; Roder & Elove, 1994; Sosnick et al., 1994). Elove et al. (1994) have recently proposed a kinetic scheme in which cyt *c* folding at pH 7 proceeds along the pathway $U \rightarrow I^H \rightarrow I^* \rightarrow N$. In this scheme, U is a collection of unfolded molecules in which the heme is ligated by His 18 and another strong ligand such as histidine or methionine. The I^H intermediate, formed on a timescale of 20 ms, possesses structured N- and C-terminal helices together with heme ligation to His 18 and a non-native histidine side chain (26 or 33). The I* intermediate, which most closely resembles the A-state, forms with a time constant of 500 ms. This intermediate retains His 18 coordination to the heme but lacks a second intramolecular axial ligand, possesses near native helical structure and Trp 59 fluorescence quenching, but shows disorder in the minor helical regions and in the Trp 59 side-chain orientation (Elove et al., 1994). The final stage involves Met 80 ligation to the heme, which completes the folding process in approximately 10 s (Myer, 1984; Elove et al., 1994). It is possible to bypass the I^H intermediate by initiating cyt *c* refolding at pH 5, where the non-native axial ligands become protonated and, in this case, I* is formed with a time constant of 15–30 ms (Elove et al., 1991). Non-native histidine ligation therefore acts as a kinetic trap that prevents the cyt *c* molecules from quickly reaching the structured I* intermediate which precedes formation of the native fold. However, differences in the kinetic behavior of I* and the A-state have been found in recent experiments by Sosnick et al. (1994), in which folding from the A-state to the native configuration occurred within the dead time of the mixing apparatus (<3 ms), which is approximately 1,000-fold faster than the formation of N from I*. This difference probably arises from incorrectly folded *cis*-proline isomers in the I* intermediate, especially at positions 71 and 76, which are close to the Met 80 ligand (Wood et al., 1988; Roder & Elove, 1994). The equilibrium conditions used to create the A-state favor the formation of *trans*-proline isomers, which permits rapid refolding to the native state.

Materials and methods

Molecular graphics

Molecular graphics studies utilized the X-ray structure coordinates provided by Professor Gary Brayer of the University of British Columbia (Bushnell et al., 1990). Coordinates were displayed on a Silicon Graphics IRIS workstation running Insight II software (Biosym, version 2.1.0). Hydrogen atoms were added to the N_1 atom of Trp 59 and the O atoms of tyrosine side chains (residues 48, 67, 74, and 97) to investigate hydrogen bonding interactions. Because the phenolic hydrogen position is not uniquely defined, the torsional angle about the CO bond was adjusted to maximize hydrogen bonding interactions by minimizing the distance between donor and acceptor atoms.

Sample preparation

Horse heart cyt *c* (type VI) was purchased from Sigma Chemical Co. A small quantity of potassium ferricyanide was added to a 4-mg/mL stock solution of cyt *c* in deionized water to con-

vert residual ferrocytochrome *c* to the oxidized form. The sample was dialyzed overnight until no residual ferricyanide was detected. The cyt *c* stock solution was diluted to the required concentration for RR experiments: 2 mg/mL for 406.7- and 230-nm laser excitation or 1 mg/mL for 200-nm experiments. The N-state was prepared at pH 6.5 in the presence of 1.5 M NaCl, and conversion to the A-state was achieved by lowering the pH to 2.2. These conditions were chosen to correspond to the NMR study of Jeng et al. (1990). The pH titration curve, monitored by the increase of absorbance at 394 nm, was identical to that reported by Jeng et al. (1990), where the sigmoidal shape of the transition curve and the isosbestic point at 406 nm are characteristic of a two-state transition. The addition of 0.15 M $NaClO_4$, required for an intensity standard in ultraviolet resonance Raman spectra, had no observable effect on the pH titration curve or the Raman spectra. Samples of the N- and A-states prepared with NaCl concentrations of 0.5, 1.0, and 1.5 M showed identical spectral properties. The unfolded protein (U-state) was prepared at pH 2.0 in H_2O in the absence of NaCl and $NaClO_4$, and the pH titration curve was identical to that reported by Goto et al. (1993). Absorption spectra were recorded on a UV/visible spectrometer (Hewlett Packard HP8452A) using a quartz cell with a 1-mm or 10-mm pathlength.

Visible resonance Raman spectroscopy

Visible RR spectra were obtained using 30 mW of 406.7-nm radiation from a Kr^+ laser (Coherent Innova 100). The samples were contained in a spinning NMR tube and illuminated in a 135° backscattering geometry. The scattered radiation was dispersed by a Spex double monochromator with a resolution of 4 cm^{-1} and detected by a photomultiplier tube (Hamamatsu). Data points were collected at 1-cm^{-1} intervals with 2 s accumulation per point, resulting in a total collection time of 50 min, and the data shown are the sum of three scans. Sample integrity was monitored by UV/visible absorption before and after laser irradiation and by comparison of spectra taken at earlier and later times: photoreduction of the protein can be detected by a red shift of the absorption maximum and the presence of an ca. 10 cm^{-1} downshifted component for the ν_4 mode. Sample degradation was observed for the U-state and the sample was consequently changed for each scan. Wavenumber values were calibrated using the band positions for indene in two spectral windows (300–800 and 1,300–1,700 cm^{-1}), and reported peak positions are accurate to ±1 cm^{-1}.

Ultraviolet resonance Raman spectroscopy

UVRR spectra were obtained using the output of an excimer-pumped dye laser (Lambda Physik LPX130/FL3002) operating at 300 Hz (Su et al., 1990; Austin et al., 1993b). The 230-nm radiation was generated by frequency doubling the output of coumarin 460 dye using a BBOI crystal. Because production of 200-nm radiation was not possible by direct output doubling, sum frequency generation was used in which the 600-nm fundamental of rhodamine B dye was mixed with its second harmonic, obtained using a BBOI crystal, in a second BBOII crystal to generate 200 nm. The UV radiation was focused, using a 135° backscattering geometry, onto the surface of a flowing sample guided between two wires and recirculated using a peristaltic pump with a 3–4-mL sample volume. The Raman-scattered light was collected by a Cassegrain mirror, dispersed using a 1.27-m Spex monochromator equipped with a 3,600-grooves/mm holographic grating (American Holographic) and detected using an image-intensified diode array (Princeton Instruments). Raman spectra were collected using 0.3 mW average laser power and are the sum of three 10-min accumulations. Sample degradation during accumulation was not observed, as monitored by pairwise subtraction of the spectra to give a flat baseline. The spectrometer response was determined by a standard deuterium lamp and used to correct the spectral intensities. Spectra were processed using Labcalc software (Galactic Industries Corp.). Wavenumber calibration of the spectra was achieved using the known wavenumber values for the Raman spectra of ethanol, where wavenumber shifts achieved with the same calibration have an accuracy of ±1 cm^{-1}, but absolute wavenumbers have an estimated accuracy of ±2 cm^{-1}. Curve fitting of the spectra was accomplished using Labcalc software using a minimal number of 50% Lorentzian/Gaussian bands with constrained bandwidths.

Acknowledgments

We thank Professor Gary Brayer of the University of British Columbia for providing the X-ray structural coordinates of horse heart cytochrome *c* and Beth Villafranca for assistance in making Figure 10. This research was supported by NIH grant GM25158.

References

Asher SA, Schuster TM. 1979. Resonance Raman examination of axial bonding and spin-state equilibria in metmyoglobin hydroxide and other heme derivatives. *Biochemistry 18*:5377–5387.

Austin JC, Jordan T, Spiro TG. 1993a. Ultraviolet resonance Raman studies of proteins and related model compounds. In: Hester, RE, Clark RJH, eds. *Advances in spectroscopy, vol 20A: Biomolecular spectroscopy*. New York: John Wiley & Sons. pp 55–127.

Austin JC, Rodgers KRR, Spiro TG. 1993b. Protein structure from ultraviolet resonance Raman spectroscopy. *Methods Enzymol 226*:374–396.

Baker EN, Hubbard RE. 1984. Hydrogen bonding in globular proteins. *Prog Biophys Mol Biol 44*:97–179.

Berghuis AM, Guillemette JG, McLendon G, Sherman F, Smith M, Brayer GD. 1994a. The role of a conserved internal water molecule and its associated hydrogen bond network in cytochrome *c*. *J Mol Biol 236*:786–799.

Berghuis AM, Guillemette JG, Smith M, Brayer GD. 1994b. Mutation of tyrosine-67 to phenylalanine in cytochrome *c* significantly alters the local heme environment. *J Mol Biol 235*:1326–1341.

Bren KL, Gray HB. 1993. Structurally engineered cytochromes with novel ligand binding sites: Oxy and carbonmonoxy derivatives of semisynthetic horse heart Ala 80 cytochrome *c*. *J Am Chem Soc 115*:10382–10383.

Bushnell GW, Louie GV, Brayer GD. 1990. High-resolution three-dimensional structure of horse heart cytochrome *c*. *J Mol Biol 214*:585–595.

Bychkova VE, Ptitsyn OB. 1993. The molten globule in vitro and in vivo. *Chemtracts—Biochem Mol Biol 4*:133–163.

Carey PD. 1982. *Biochemical applications of Raman and resonance Raman spectroscopies*. New York: Academic Press.

Cartling B. 1988. Cytochrome *c*. In: Spiro TG, ed. *Biological applications of resonance Raman spectroscopy, vol 3*. New York: John Wiley & Sons. pp 217–248.

Christensen H, Pain RH. 1991. Molten globule intermediates and protein folding. *Eur Biophys J 19*:221–229.

Christensen H, Pain RH. 1994. The contribution of the molten globule. In: Pain RH, ed. *Mechanisms of protein folding*. Oxford: IRL Press. pp 55–79.

Cho N, Song S, Asher SA. 1994. UV resonance Raman and excited-state relaxation rate studies of hemoglobin. *Biochemistry 33*:5932–5941.

Chyan CH, Wormald CW, Dobson CM, Evans PA, Baum JA. 1993. Struc-

ture and stability of the molten globule state of Guinea-pig α-lactalbumin: A hydrogen exchange study. *Biochemistry 32*:5681–5691.
Copeland R, Spiro TG. 1985. Ultraviolet resonance Raman spectra of cytochrome *c* conformational states. *Biochemistry 24*:4960–4968.
Dickerson RE, Timkovich R. 1975. Cytochromes *c*. In: Boyer PD, ed. *The enzymes, vol XI*. New York: Academic Press. pp 397–547.
Dill KA, Shortle D. 1991. Denatured states of proteins. *Annu Rev Biochem 60*:795–826.
Dumont ME, Corin AF, Campbell GA. 1994. Noncovalent bonding of heme induces a compact apocytochrome *c* structure. *Biochemistry 33*:7368–7378.
Dyson HJ, Beattie JK. 1982. Spin state and unfolding equilibria of ferricytochrome *c* in acidic solutions. *J Biol Chem 257*:2267–2273.
Elove GA, Bhuyan AK, Roder H. 1994. Kinetic mechanism of cytochrome *c* folding: Involvement of the heme and its ligands. *Biochemistry 33*:6925–6935.
Elove GA, Chaffotte AF, Roder HA, Goldberg ME. 1991. Early steps in cytochrome *c* folding probed by time-resolved circular dichroism and fluorescence spectroscopy. *Biochemistry 31*:6876–6883.
Elove GA, Roder HA. 1991. Structure and stability of cytochrome *c* folding intermediates. In: Georgiou G, de Bernadez-Clark E, eds. *Protein Refolding: ACS Symposium Series 470*. Washington, DC: American Chemical Society Press. pp 50–63.
Englander SW, Mayne L. 1992. Protein folding studied using hydrogen-exchange labeling and two-dimensional NMR. *Annu Rev Biophys Biomol Struct 21*:243–265.
Fink A, Calciano L, Goto Y, Palleros DR. 1990. Acid denatured states of proteins. *Curr Res Protein Chem 3*:417–424.
Fisher WR, Taniuchi H, Anfinsen CB. 1973. On the role of the heme in the formation of the structure of cytochrome *c*. *J Biol Chem 248*:3188–3195.
Fodor SPA, Copeland RA, Grygon CA, Spiro TG. 1989. Deep-ultraviolet Raman excitation profiles and vibronic scattering mechanisms of phenylalanine, tyrosine and tryptophan. *J Am Chem Soc 111*:5509–5518
Fredericks ZL, Pielak GJ. 1993. Exploring the interface between the N- and C-terminal helices of cytochrome *c* by random mutagenesis within the C-terminal helix. *Biochemistry 32*:929–936.
Goto Y, Calciano LJ, Fink AL. 1990a. Acid-induced folding of proteins. *Proc Natl Acad Sci USA 87*:573–577.
Goto Y, Hagihara Y, Hamada D, Hoshino M, Nishii I. 1993. Acid-induced unfolding and refolding transitions of cytochrome *c*: A three-state mechanism in H_2O and D_2O. *Biochemistry 32*:11878–11885.
Goto Y, Nishikiori S. 1991. Role of electrostatic repulsion in the acidic molten globule of cytochrome *c*. *J Mol Biol 222*:679–686.
Goto Y, Takahashi N, Fink AL. 1990b. Mechanism of acid-induced folding of proteins. *Biochemistry 29*:3480–3488.
Hagihara Y, Tan Y, Goto Y. 1994. Comparison of the conformational stability of the molten globule and native states of horse heart cytochrome *c*. *J Mol Biol 237*:336–348.
Hamada D, Hoshino M, Kataoka M, Fink AL, Goto Y. 1993. Intermediate conformational states of apocytochrome *c*. *Biochemistry 32*:10351–10358.
Harada I, Miura T, Takeuchi H. 1986. Origin of the doublet at 1360 and 1340 cm^{-1} in the Raman spectra of tryptophan and related compounds. *Spectrochim Acta 42A*:307–312.
Harada I, Takeuchi H. 1986. Raman and ultraviolet resonance Raman spectra of proteins and related compounds. In: Clark RJH, Hester RE, eds. *Spectroscopy of biological systems*. New York: John Wiley. pp 113–175.
Hu S, Shiau FY, Smith KA, Spiro TG. 1993. Complete assignment of cytochrome *c* resonance Raman spectra via enzymatic reconstitution with isotopically labeled hemes. *J Am Chem Soc 115*:12446–12458.
Hughson FM, Wright PE, Baldwin RL. 1990. Structural characterization of a partially folded apomyoglobin intermediate. *Science 249*:1544–1548.
Ikeguchi M, Kuwajima K, Mitani M, Sugai S. 1986. Evidence for identity between the equilibrium folding intermediate and a transient folding intermediate: A comparative study of the folding reactions of α-lactalbumin and lysozyme. *Biochemistry 25*:6965–6972.
Ippolito JA, Alexander RS, Christianson DW. 1990. Hydrogen bond stereochemistry in protein structure and function. *J Mol Biol 215*:457–471.
Jayaraman V, Rodgers KR, Mukerji I, Spiro TG. 1993. R and T states of fluoromethemoglobin studied by ultraviolet resonance Raman spectroscopy. *Biochemistry 32*:4547–4551.
Jeng MF, Englander SW. 1991. Stable submolecular folding units in a non-compact form of cytochrome *c*. *J Mol Biol 221*:1045–1061.
Jeng MF, Englander SW, Elove GA, Wand JA, Roder H. 1990. Structural description of acid-denatured cytochrome *c* by hydrogen exchange and 2D NMR. *Biochemistry 29*:10433–10437.
Jennings PA, Wright PE. 1993. Formation of a molten globule intermediate early in the kinetic folding pathway of apomyoglobin. *Science 262*:892–896.
Johnson WC. 1990. Protein secondary structure and circular dichroism: A practical guide. *Proteins Struct Funct Genet 7*:205–214.
Jordan T, Spiro TG. 1994. Enhancement of C_α hydrogen vibrations in the resonance Raman spectra of amides. *J Raman Spectrosc 25*:537–543.
Kataoka M, Hagigara Y, Mihara K, Goto Y. 1993. Molten globule of cytochrome *c* studied by small angle X-ray scattering. *J Mol Biol 229*:591–596.
Kitagawa T, Nagai K. 1979. Quaternary structure-induced photoreduction of haem of haemoglobin. *Nature 281*:503–504.
Krimm S, Bandekar J. 1986. Vibrational spectroscopy and conformation of peptides, polypeptides, and proteins. *Adv Protein Chem 38*:181–364.
Kuroda Y. 1993. Residual helical structure in the C-terminal fragment of cytochrome *c*. *Biochemistry 32*:1219–1224.
Kuroda Y, Kidokoro S, Wada A. 1992. Thermodynamic characterization of cytochrome *c* at low pH. *J Mol Biol 223*:1139–1153.
Kuwajima K. 1989. The molten globule state as a clue for understanding the folding and cooperativity of globular-protein structure. *Proteins Struct Funct Genet 6*:87–103.
Li XY, Czernuszewicz R, Kincaid JR, Spiro TG. 1991. Consistent porphyrin forcefield 3: Out-of-plane modes in the resonance Raman spectra of planar and ruffled nickel octaethylporphyrin. *J Am Chem Soc 111*:7012–7023.
Liu GY, Grygon CA, Spiro TG. 1989. Ionic strength dependence of cytochrome *c* structure and Trp-59 H/D exchange from ultraviolet resonance Raman spectroscopy. *Biochemistry 28*:5046–5050.
Makinen MW, Churg AK. 1983. Structural and analytic aspects of the electronic spectra of hemeproteins. In: Lever ABP, Gray HB, eds. *Iron porphyrins, part 1*. Reading, Massachusetts: Addison-Wesley. pp 141–325.
Miura T, Takeuchi H, Harada I. 1988. Characterization of individual tryptophan side chains in proteins using Raman spectroscopy and hydrogen-deuterium exchange *Biochemistry 27*:88–94.
Miura T, Takeuchi H, Harada I. 1989. Tryptophan Raman bands sensitive to hydrogen bonding and side-chain conformation. *J Raman Spectrosc 20*:667–671.
Myer YP. 1978. Circular dichroism spectroscopy of hemoproteins. *Methods Enzymol 54*:249–284.
Myer YP. 1984. Ferricytochrome *c*. Refolding and the methionine 80-sulfur-iron linkage. *J Biol Chem 259*:6127–6133.
Myer YP, Pande A. 1978. Circular dichroism studies of hemoproteins and heme models. In: Dolphin D, ed. *The porphyrins, vol IIIA*. New York: Academic Press. pp 271–322.
Myer YP, Saturno AF. 1991. Horse heart ferricytochrome *c*: Conformation and heme configuration of high ionic strength acidic forms. *J Protein Chem 10*:481.
Nishii I, Kataoka F, Tokunaga, Goto Y. 1994. Cold denaturation of the molten globule state of apomyoglobin and a profile for protein folding. *Biochemistry 33*:4903–4909.
Ponder JW, Richards FM. 1987. Tertiary templates for proteins. *J Mol Biol 193*:775–791.
Ptitsyn OB. 1986. Protein folding: Hypotheses and experiments. *J Protein Chem 6*:273–293.
Ptitsyn OB. 1993. The molten globule state. In: Creighton TE, ed. *Protein folding*. New York: W.H. Freeman. pp 243–300.
Roder H, Elove GA. 1994. Early stages of protein folding. In: Pain RH, ed. *Mechanisms of protein folding*. Oxford: IRL Press. pp 26–54.
Roder H, Elove GE, Englander SW. 1988. Structural characterization of folding intermediates in cytochrome *c* by H-exchange labelling and proton NMR. *Nature 335*:700–704.
Rodgers KRR, Su C, Subramanian S, Spiro TG. 1992. Hemoglobin R → T structural dynamics from simultaneous monitoring of tyrosine and tryptophan time-resolved UV resonance Raman signals. *J Am Chem Soc 114*:3697–3709.
Smulevich G. 1993. Structure–function relationships in peroxidases via resonance Raman spectroscopy and site-directed mutagenesis: Cytochrome *c* peroxidase. In: Hester RE, Clark RJH, eds. *Advances in spectroscopy, vol 20A: Biomolecular spectroscopy*: New York: John Wiley. pp 163–193.
Smulevich G, Bjerrum MI, Gray HB, Spiro TG. 1994. Active site structure of the semisynthetic Cys 80 mutant of cytochrome *c*. *Inorg Chem 33*: 4629–4634.
Song S, Asher SA, Krimm S, Shaw KD. 1991. Ultraviolet resonance Raman studies of *trans* and *cis* peptides: Photochemical consequences of the twisted π^* excited state. *J Am Chem Soc 113*:1155–1163.
Sosnick TR, Mayne L, Hiller R, Englander SW. 1994. The barriers in protein folding. *Nature Struct Biol 1*:149–156.
Spiro TG. 1983. The resonance Raman spectroscopy of metalloporphyrins and heme proteins. In: Lever ABP, Gray HB, eds. *Iron porphyrins, part II*. Reading, Massachusetts: Addison-Wesley Publishing Company. pp 89–159.

Spiro TG. 1985. Resonance Raman spectroscopy as a probe of heme protein structure and dynamics. *Adv Protein Chem 37*:111–159.

Spiro TG, Li XY. 1988. Resonance Raman spectroscopy of metalloporphyrins. In: Spiro TG, ed. *Biological applications of resonance Raman spectroscopy, vol 3*. New York: John Wiley. pp 1–37.

Stellwagen E, Rysavy R, Babul J. 1972. The conformation of horse heart apocytochrome *c*. *J Biol Chem 247*:8074–8077.

Stigter D, Alonso DOV, Dill KA. 1991. Protein stability: Electrostatics and compact denatured states. *Proc Natl Acad Sci USA 88*:4176–4180.

Strekas TC, Spiro TG. 1974. Resonance-Raman evidence for an anomalous heme structure in cytochrome *c'* from *Rhodopseudomonas palustris*. *Biochim Biophys Acta 351*:237–235.

Su C, Wang Y, Spiro TG. 1990. Saturation effects on ultraviolet resonance Raman intensities: Excimer/YAG laser comparisons and aromatic amino acid cross-sections. *J Raman Spectrosc 21*:435–440.

Takeuchi H, Watanabe N, Satoh Y, Harada I. 1989. Effects of hydrogen bonding on the tyrosine Raman bands in the 1300–1150 cm^{-1} region. *J Raman Spectrosc 20*:233–237.

Timkovich R. 1979. Cytochrome *c*: The architecture of a protein–porphyrin complex. In: Dolphin D, ed. *The porphyrins, vol VII*. New York: Academic Press. pp 241–294.

Tu A. 1982. *Raman spectroscopy in biology: Principles and applications*. New York: John Wiley.

Wand AJ, Englander SW. 1986. Two-dimensional ^1H NMR studies of cytochrome *c*: Assignment of the N-terminal helix. *Biochemistry 25*:1100–1106.

Wand AJ, Roder H, Englander SW. 1986. Two-dimensional ^1H NMR studies of cytochrome *c*: Hydrogen exchange in the N-terminal helix. *Biochemistry 25*:1107–1114.

Wang Y, Purrello R, Jordan T, Spiro TG. 1991. UVRR spectroscopy of the peptide bond. 1. Amide S, a nonhelical structure marker, is a $C_\alpha H$ bending mode. *J Am Chem Soc 113*:6359–6368.

Wood LC, White TB, Ramdas L, Nall BT. 1988. Replacement of a conserved proline eliminates the absorbance-detected slow folding phase of iso-2-cytochrome *c*. *Biochemistry 27*:8562–8568.

Wu LC, Laub PB, Elove GA, Carey J, Roder H. 1993. A noncovalent peptide complex as a model for an early folding intermediate of cytochrome *c*. *Biochemistry 32*:10271–10276.